



Article

# Comparison of Erosion Behavior and Particle Contamination in Mass-Production $\text{CF}_4/\text{O}_2$ Plasma Chambers Using $\text{Y}_2\text{O}_3$ and $\text{YF}_3$ Protective Coatings

Tzu-Ken Lin <sup>1</sup>, Wei-Kai Wang <sup>2</sup>, Shih-Yung Huang <sup>3</sup>, Chi-Tsung Tasi <sup>1</sup> and Dong-Sing Wu <sup>1,4,\*</sup>

<sup>1</sup> Department of Materials Science and Engineering, National Chung Hsing University, Taichung 40227, Taiwan; alexlin19781121@hotmail.com (T.-K.L.); d100066018@mail.nchu.edu.tw (C.-T.T.)

<sup>2</sup> Department of Materials Science and Engineering, Da-Yeh University, Changhua 51591, Taiwan; wk@mail.dyu.edu.tw

<sup>3</sup> Department of Industrial Engineering and Management, Da-Yeh University, Changhua 51591, Taiwan; syh@mail.dyu.edu.tw

<sup>4</sup> Center for Advanced Industry Technology and Precision Processing, National Chung Hsing University, Taichung 40227, Taiwan

\* Correspondence: dsw@nchu.edu.tw; Tel.: +886-4-2284-0500 (ext. 714); Fax: +886-4-2285-5046

Academic Editor: Melanie Ramiasa

Received: 15 June 2017; Accepted: 11 July 2017; Published: 14 July 2017

**Abstract:** Yttrium fluoride ( $\text{YF}_3$ ) and yttrium oxide ( $\text{Y}_2\text{O}_3$ ) protective coatings prepared using an atmospheric plasma spraying technique were used to investigate the relationship between surface erosion behaviors and their nanoparticle generation under high-density plasma ( $10^{12}$ – $10^{13}$   $\text{cm}^{-3}$ ) etching. As examined by transmission electron microscopy, the  $\text{Y}_2\text{O}_3$  and  $\text{YF}_3$  coatings become oxyfluorinated after exposure to the plasma, wherein the yttrium oxyfluoride film formation was observed on the surface with a thickness of 5.2 and 6.8 nm, respectively. The difference in the oxyfluorination of  $\text{Y}_2\text{O}_3$  and  $\text{YF}_3$  coatings could be attributed to Y–F and Y–O bonding energies. X-ray photoelectron spectroscopy analyses revealed that a strongly fluorinated bonding (Y–F bond) was obtained on the etched surface of the  $\text{YF}_3$  coating. Scanning electron microscopy and energy dispersive X-ray diffraction analysis revealed that the nanoparticles on the 12-inch wafer are composed of etchant gases and  $\text{Y}_2\text{O}_3$ . These results indicate that the  $\text{YF}_3$  coating is a more erosion-resistant material, resulting in fewer contamination particles compared with the  $\text{Y}_2\text{O}_3$  coating.

**Keywords:** yttrium fluoride ( $\text{YF}_3$ ); yttrium oxide ( $\text{Y}_2\text{O}_3$ ); atmospheric plasma spraying (APS); particle contamination

## 1. Introduction

Silicon-based ceramics have been extensively used in semiconductor plasma processing equipment as plasma-facing materials, due to their hardness, high wear resistance, dielectric strength, high corrosion resistance, and chemical stability [1,2]. They are used mainly as a shield to protect the ceramic parts inside etchers or chemical vapor deposition reactor chambers from corrosion caused by fluorocarbon corrosive gases such as  $\text{CF}_4$ ,  $\text{CHF}_3$ ,  $\text{C}_4\text{F}_6$ , and  $\text{C}_2\text{F}_6$  [3–5]. These materials interact with plasma and are eroded, resulting in the production of contaminant particles on the wafer. As integrated circuits continue to scale down with wider use of high-density plasma for wafer processing, the particles generated in the plasma processing equipment cause serious problems, such as short current in integration circuit and lower production yield [6,7]. In order to solve this problem, yttrium oxide ( $\text{Y}_2\text{O}_3$ ) was adopted as plasma-facing inner wall materials in plasma processing equipment because their plasma erosion resistance values are much higher than those of conventional

SiO<sub>2</sub> coatings [8–10]. Mass-production factories have found that the Y<sub>2</sub>O<sub>3</sub> inner walls have problems with significant erosion and particle generation [11]. Under fluorine-based plasma processing, a thin top carbonaceous polymer reaction layer has been identified depending on the etching conduction and the etched materials [12–14]. The polymer layer thickness is determined using polymer deposition and its removal rate, and consumption rate in substrate etching. This polymer layer etching rate is affected by the plasma incident ion kinetic energy. Some volatile etching products are produced during the etching process, such as carbon oxide, carbon oxyfluorides, and silicon fluorides [15]. Unlike silicon-based materials, the yttrium-based material etching mechanism is not fully understood. Yttrium fluoride (YF<sub>3</sub>) coatings have recently attracted substantial attention because of their high plasma erosion resistance, preventing the generation of fluoride particles on the chamber wall surface, reducing particulate contamination [16]. Thus, the YF<sub>3</sub> coating might be a new plasma-facing material that produces fewer contamination particles. The Y<sub>2</sub>O<sub>3</sub> and YF<sub>3</sub> coatings were deposited using atmospheric plasma spraying (APS). In this study, the mechanism of formation of yttrium oxyfluoride film and their particle trajectories in industrial plasma processing tools have been examined. Moreover, we compared the etching behavior of Y<sub>2</sub>O<sub>3</sub> and YF<sub>3</sub> coatings and their compounds under fluorocarbon plasma. The surface morphology, chemical reactions on the etched surface, microstructure, and particle contaminations of Y<sub>2</sub>O<sub>3</sub> and YF<sub>3</sub> coatings were investigated.

## 2. Materials and Methods

Commercially available YF<sub>3</sub> powders (25–50 μm, 99.99%, Shin-Etsu Chemical, Tokyo, Japan) and Y<sub>2</sub>O<sub>3</sub> powders (25–50 μm, 99.99%, Shin-Etsu Chemical, Tokyo, Japan) were used as the spraying materials. YF<sub>3</sub> and Y<sub>2</sub>O<sub>3</sub> coatings were prepared using APS with an F4-MB plasma gun (Sulzer Metco, Orelikon, Pfaeffikon, Switzerland). An alloy aluminum (A6061) substrate was used for the experiment. The specimen had a size of 400 mm<sup>2</sup> and a thickness of 20 mm. Before APS, the substrate was treated with sandblasting. The sandblasting material was SiO<sub>2</sub>. Acetone was used to clean the substrate. The stand-off distance was adjusted to 10 cm. The Ar and H<sub>2</sub> gas cylinders were opened when the air compressor was initiated. The Ar flow rate, H<sub>2</sub> flow rate, system voltage, gun movement rate, and feed rate were set to 45 L/min, 6 L/min, 50 V, 10 cm/s, and 15 g/min, respectively. The YF<sub>3</sub> and Y<sub>2</sub>O<sub>3</sub> spraying parameters are shown in Table 1. The erosion behaviors of both protective coatings were performed using an inductively coupled plasma (ICP) etcher (LAM 2300 Metal) under the routine plasma etching process; i.e., the same bias power and processing gases (CF<sub>4</sub> and O<sub>2</sub>). High-density CF<sub>4</sub>/O<sub>2</sub> plasma with electron densities on the order of 10<sup>12</sup> to 10<sup>13</sup> cm<sup>−3</sup> has been produced. Figure 1 shows a schematic diagram of the ICP etcher system employed in this study. The etch process details are shown in Table 2. Three-hundred millimeter blanket wafers with chemical vapor deposition titanium nitride layer/Si-substrate were prepared to evaluate the integrated circuit defective performance after dry etching process measured by Surfscan SP3 (Surfscan SP3, KLA-Tencor Corporation, Milpitas, CA, USA).

The surface morphology, microstructure, and elemental analysis of these coating samples were conducted using scanning electron microscopy (SEM, S-3000H, Hitachi, Tokyo, Japan) coupled with energy dispersive X-ray diffraction (EDX) and transmission electron microscopy (TEM, H-600, Hitachi, Tokyo, Japan). The composition of these samples were examined by X-ray photoelectron spectroscopy (XPS, PHI 5000 VersaProbe, ULVAC-PHI, Kanagawa, Japan) using a monochromatic Al Kα X-ray source at a passing energy of 20 eV with a spot size of 650 μm, then the sample surface was etched using focused argon ions sputtering to investigate the chemical compositional depth profile (ThermoScientific K-Alpha). A fitting software program (Thermo Fisher Scientific, Inc., Waltham, MA, USA) was used to deconvolute the photoelectron spectrum resulting from the core energy levels of Yttrium 3d states to estimate the contributions from bonding with fluorine elements.

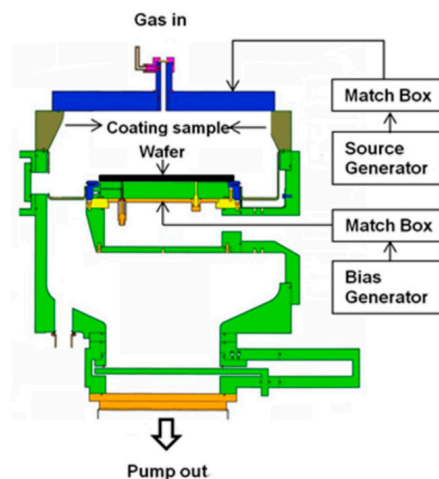


**Figure 1.** Schematic illustration of the cross section of inductively coupled plasma (ICP) etching tool.

**Table 1.** Spraying parameters for coatings made of  $Y_2O_3$  and  $YF_3$ .

Condition	$Y_2O_3$	$YF_3$
Primary gas flow rate (L/min)	45	45
Secondary current (L/min)	6	6
Gun moving rate (cm/s)	10	10
System voltage (V)	50	50
Gun power (kW)	15	15
Stand-off (cm)	10	10

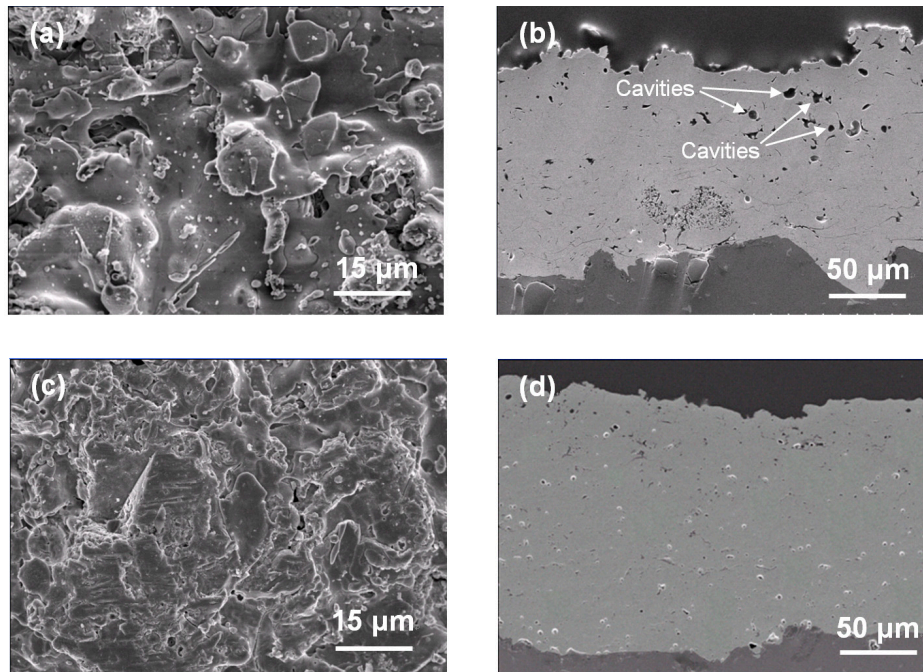
**Table 2.** Plasma etching parameters for  $Y_2O_3$  and  $YF_3$  coatings.

Condition	$Y_2O_3$	$YF_3$
RF source power (W)	1300	1300
RF bias power (W)	500	500
Chamber pressure (Pa)	1.06	1.06
$CF_4:O_2$ (sccm)	30:5	30:5
Etching time (min)	60	60

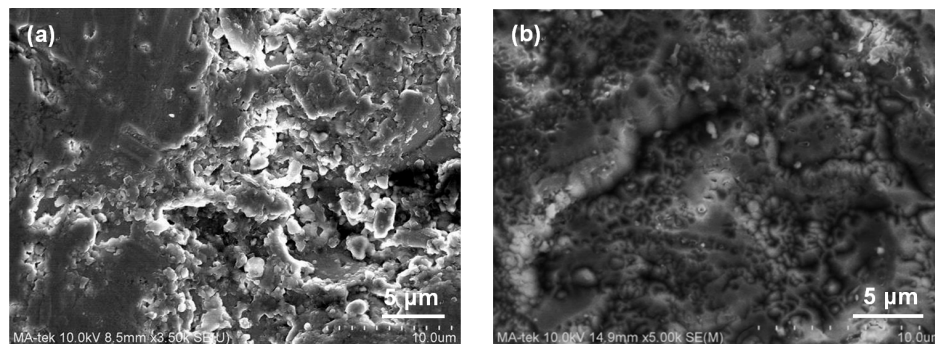
### 3. Results and Discussion

Figure 2 shows the surface and cross-sectional SEM images of  $Y_2O_3$  and  $YF_3$  coatings under 15 kW plasma spraying powers. Figure 2a shows the  $Y_2O_3$  coating with poor surface roughness with laminar morphology. A horizontal crack and large cavities (within the size range of 5–10  $\mu m$ ) are also observed (Figure 2b). Dense  $YF_3$  coating layers with less porosity are shown in Figure 2c,d). Due to the small difference in thermal expansion between the  $YF_3$  coating ( $28.5 \times 10^{-6}/K$ ) and the Al substrate ( $23 \times 10^{-6}/K$ ), no cracks were observed in any  $YF_3$  coating samples. The erosion-resistance characteristics of  $Y_2O_3$  and  $YF_3$  coatings were measured after exposure to the  $CF_4/O_2$  plasma, as discussed below. Figure 3a,b show the SEM image surface microstructure of the  $Y_2O_3$  and  $YF_3$  coatings after etching in  $CF_4/O_2$  plasma for 60 min under a bias power of 500 W. There is a large difference in etched surface for both coating samples under the same etching condition. In Figure 3a, the surface of  $Y_2O_3$  coating is obviously cracked after the etching process. These  $Y_2O_3$  cracked pieces might be a particle contamination source during the wafer fabrication process. In Figure 3b, the  $YF_3$  coating is revealed to have a relatively dense and smooth surface, indicating that the erosion of  $Y_2O_3$  coating was more severe than  $YF_3$  coating after exposure to  $CF_4/O_2$  plasma. It is also consistent with our previous study regarding the film porosity [16], since the erosion resistance to  $CF_4/O_2$  plasma (chemical reaction) was enhanced by reducing film porosity [17]. From the SEM observation

results, the  $\text{YF}_3$  coating revealed that a clean and complete surface can be obtained by preventing the fluoride particles from attaching to the etching chamber sidewall after exposure to the fluorocarbon plasma during etching. Hence, the  $\text{YF}_3$  coating is more favorable for application in plasma processing equipment. Similar results were consistent with the previously reported data by Kim et al. [18].



**Figure 2.** Surface and cross-sectional SEM images of (a,b)  $\text{Y}_2\text{O}_3$  and (c,d)  $\text{YF}_3$  coating at plasma spray power of 15 kW.



**Figure 3.** SEM images after fluorocarbon plasma treatment: (a)  $\text{Y}_2\text{O}_3$  and (b)  $\text{YF}_3$  coatings.

Figure 4 shows the compositional variation with the sputtering time from the  $\text{Y}_2\text{O}_3$  and  $\text{YF}_3$  coating surfaces after exposure to the  $\text{CF}_4/\text{O}_2$  plasma by using XPS. The  $\text{Y}_2\text{O}_3$  and  $\text{YF}_3$  coating surfaces before exposure to the  $\text{CF}_4/\text{O}_2$  plasma are shown in Figure 4a,b. The carbon content found on the surface decreased abruptly with the sputtering time, indicating that the carbon polymer layer is very thin (Figure 4c,d). This thin carbon polymer layer on the etched surface was previously reported in Si-based oxide materials etched under fluorocarbon plasma [19–21]. Moreover, the fluorine was verified on both  $\text{Y}_2\text{O}_3$  and  $\text{YF}_3$  coatings and the higher fluorine content was detected on the  $\text{YF}_3$  surface (Figure 4c,d). It was found that the percentage of F atoms reached the maximum value of 35% and 48% on the  $\text{Y}_2\text{O}_3$  and  $\text{YF}_3$  coatings after etching, causing a thicker fluorination layer to appear in the  $\text{YF}_3$  specimen. This is because  $\text{YF}_3$  is a fluorine-rich compound material; hence, the chemical

composition of F atoms in the YF<sub>3</sub> coating was unchanged accompanied with the depth from the surface. The stronger YF<sub>3</sub> coating fluorination can also be confirmed by the XPS spectral analysis on etched sample surfaces.

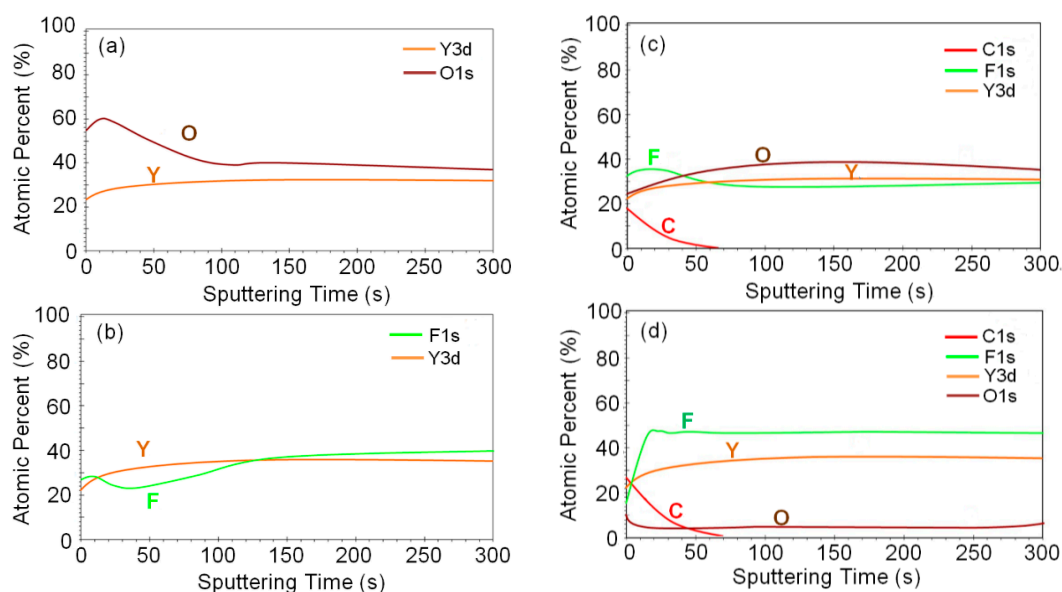
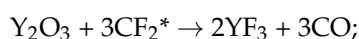
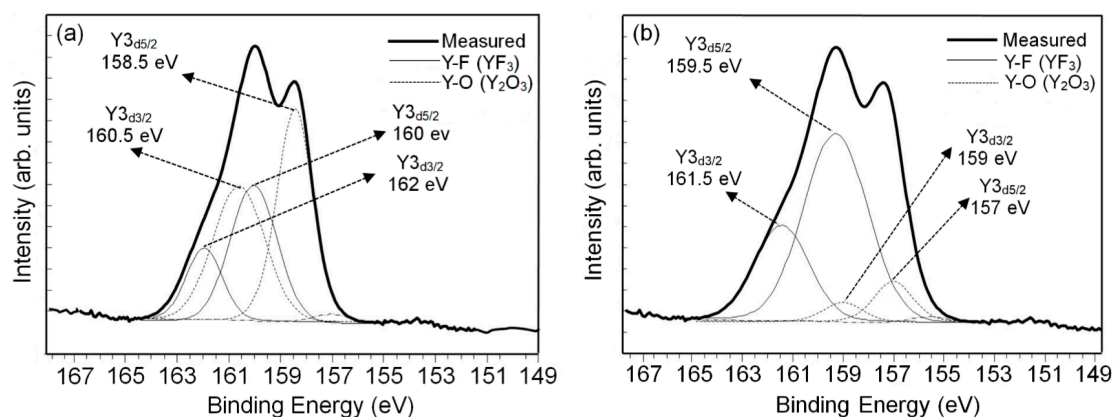


**Figure 4.** Variations of chemical compositions measured using X-ray photoelectron spectroscopy (XPS) with the sputtering time of (a,c) the Y<sub>2</sub>O<sub>3</sub> and (b,d) the YF<sub>3</sub> coatings before and after exposure to the fluorocarbon plasma.

Figure 5 represents the XPS spectra for the yttrium atoms from the (a) Y<sub>2</sub>O<sub>3</sub> and (b) YF<sub>3</sub> coating samples after CF<sub>4</sub>/O<sub>2</sub> plasma etching. In the curve-fitted XPS spectra of the Y<sub>2</sub>O<sub>3</sub> coating, two peaks mean two sources of bonding for cations from Y3d split into two Y3d<sub>5/2</sub> states (high peaks) and Y3d<sub>3/2</sub> (low peaks) [22]. In Figure 5a, the etched surface of the Y<sub>2</sub>O<sub>3</sub> coating consisted of Y3d<sub>5/2</sub> and Y3d<sub>3/2</sub>, with an intensity ratio of 3:2 and peak shift difference in the binding energy of 2 eV, according to the XPS standard [23,24]. This peak shifting to higher binding energy (located at 160 and 162 eV) could be attributed to Y–F bonding in the Y<sub>2</sub>O<sub>3</sub> sample. The higher electronegativity of fluorine (4.0) compared to that of oxygen (3.5) causes higher electron binding energy from the cation [25]. This high fluorine concentration demonstrated that the Y<sub>2</sub>O transformed into a YO<sub>x</sub>F<sub>y</sub> (x + y = 1.5) and/or YF<sub>x</sub> (x < 3) surface by the exposed fluorine-based plasma [26]. Meanwhile, the two binding energy peaks located at 158.5 and 160.5 eV correspond to a Y–O bond, resulting in a low binding energy. Figure 5b shows the YF<sub>3</sub> coating XPS spectra on the etched surface deconvoluted into four peaks, corresponding to Y–F bonding (located at 159.5 and 161.5 eV) and Y–O bonding (located at 157 and 159 eV) [27,28]. Furthermore, the intensity ratio of Y–F to Y–O peaks on the YF<sub>3</sub> coating reached 2.9, which was much higher than that of the Y–F to Y–O peak on the Y<sub>2</sub>O<sub>3</sub> coating (0.73), indicating stronger fluorination on the etched YF<sub>3</sub> coating surface. These results indicate that the YF<sub>3</sub> coating exhibited superior inherent chemical stability after fluorocarbon plasma treatment [29]. The reactions for CF<sub>4</sub>/O<sub>2</sub> plasma chemical etching of Y<sub>2</sub>O<sub>3</sub> and YF<sub>3</sub> coatings can be expressed as follows:

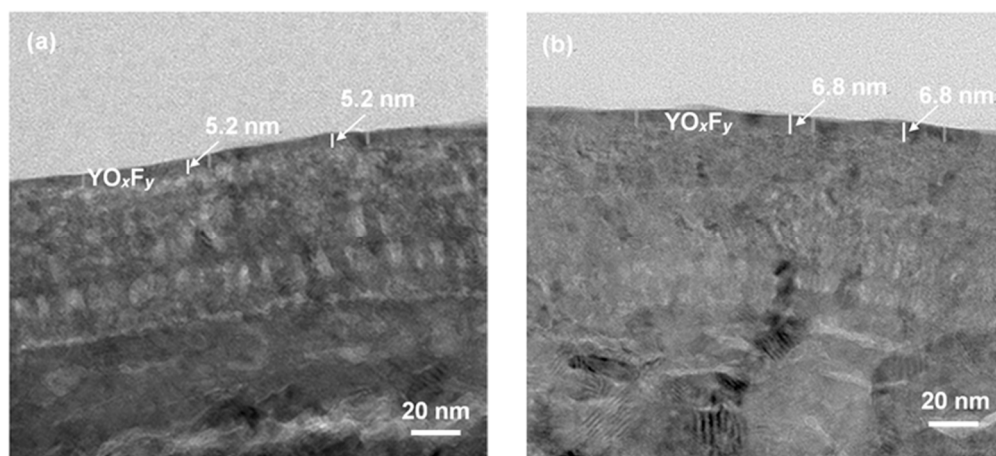


when the CF<sub>4</sub>/O<sub>2</sub> plasma chemical reaction dominates the etching process, and the chemical stability YF<sub>3</sub> might be effective in the suppression of particle generation during the etching process, as mentioned in the SEM results.



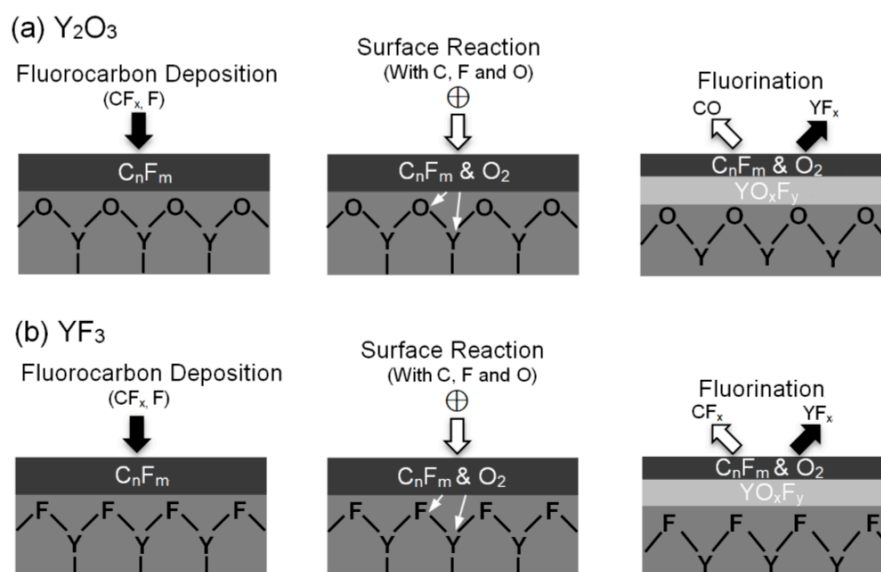
**Figure 5.** Variations of chemical compositions measured using XPS with the sputtering time of (a) the  $Y_2O_3$  and (b) the  $YF_3$  coatings after exposure to the fluorocarbon plasma.

The microstructures of both coated samples irradiated by high-density  $CF_4/O_2$  plasma were revealed by TEM. Figure 6a,b shows cross-sectional TEM micrographs of the plasma-etched  $Y_2O_3$  and  $YF_3$  coatings, respectively. A yttrium oxyfluoride ( $YO_xF_y$ ) film 5.2 nm in thickness was observed on the  $Y_2O_3$  surface, while the  $YF_3$  sample showed a thicker  $YO_xF_y$  of 6.8 nm. The slightly lesser fluorination of  $Y_2O_3$  than  $YF_3$  is explained by comparing the bonding energies of Y–O (685 KJ/mol) and Y–F (605 KJ/mol). Because the bonding energy of Y–O is higher than Y–F, it results in less-efficient reactions between the Y–O bonding and the fluorocarbon film. The formation of an oxyfluoride layer on the surface of  $Y_2O_3$  and  $YF_3$  coatings might act as a protecting layer to prevent the coating’s surface from further erosion by  $CF_4/O_2$  plasma.



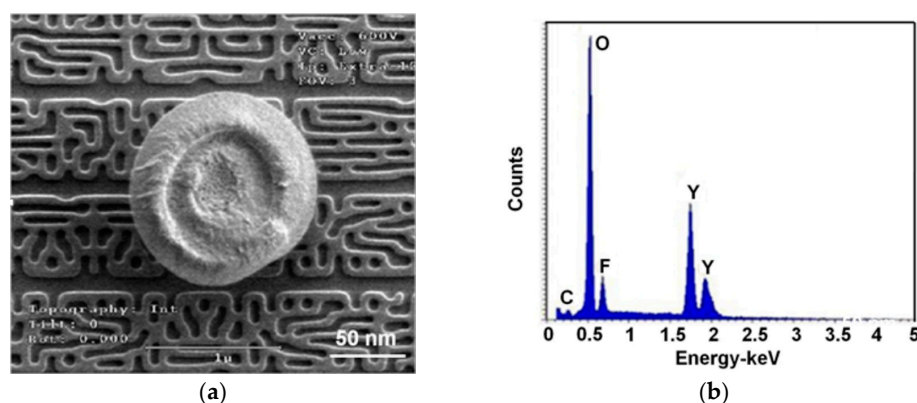
**Figure 6.** TEM microstructures of (a)  $Y_2O_3$  and (b)  $YF_3$  coatings after exposure to the fluorocarbon plasma.

Figure 7 illustrates the schematic formation mechanism of  $YO_xF_y$  on  $Y_2O_3$  and  $YF_3$  surfaces. The procedure of  $YO_xF_y$  formation on the  $Y_2O_3$  and  $YF_3$  surfaces is as follows: the first step is deposition of the fluorocarbon film by the adsorption of  $CF_x$  radicals on these two coatings’ sample surfaces. The second step is carbon reactions with oxygen (Y–O) and fluorine (Y–F) to form volatile CO and  $CF_x$ , resulting in the decomposition of the Y–O and Y–F bondings. Subsequently, the  $YO_xF_y$  film is formed in the  $Y_2O_3$  and  $YF_3$  coatings surface (third step), whereas a part of  $YF_x$  may desorb from the coating surface. Similar reactions and formation of  $YO_xF_y$  were also investigated previously [30,31]. It is believed that the  $YO_xF_y$  layer is effective in reducing practical generation and thus contamination of the integrated circuit [32].



**Figure 7.** Schematic illustration of yttrium oxyfluoride film deposition behavior on (a)  $Y_2O_3$  and (b)  $YF_3$  coatings.

One of the prime concerns of production yields is the particles generated from the plasma processing equipment, resulting in open- or short-circuits. We have investigated the possible particles generated during the etching process using an in-situ particle monitoring system which can detect the particle trajectories. Figure 8a shows an SEM image of a typical particle observed on the wafer surface. The circular particle is composed of etchant gases and a  $Y_2O_3$ -coated chamber wall after exposed to  $CF_4/O_2$  plasma—it can be called a partial etch defect. An EDX analysis was carried out to clarify the particle compositions. As shown in Figure 8b, it was found that the flaking particles were composed mainly of yttrium, oxide, and fluoride elements, indicating the particle source from the  $Y_2O_3$  coating. Therefore, the  $YF_3$  coating can behave as a new plasma-facing material that produces fewer contamination particles.



**Figure 8.** (a) SEM image of a circular particle and (b) energy dispersive X-ray diffraction (EDX) analysis results of circular particle.

#### 4. Conclusions

During the plasma etching process, particles generated from the  $Y_2O_3$  and  $YF_3$  protective coatings of the ICP chamber wall were investigated in this study. The particle generation mechanism could be due to the fact that the bonding strength of Y–O was weaker than that of Y–F when the chamber-wall

surface suffered irradiation from high-density  $\text{CF}_4/\text{O}_2$  plasmas. From the SEM examination results,  $\text{YF}_3$  was also confirmed to be more robust than  $\text{Y}_2\text{O}_3$  against  $\text{CF}_4/\text{O}_2$  plasma irradiation. The  $\text{YF}_3$  coatings for the ICP etching chamber components and materials can play an important role in decreasing the extreme number of particles in the fluorine-based plasma environment.

**Acknowledgments:** This work was supported by the Ministry of Science and Technology (Taiwan) with Grant Nos. 105-2622-8-005-003-TE1 and 105-2221-E-005-059-MY3. The authors wish to express their sincere gratitude for the financial and technical support from the advanced Industry Technology Centre of National Chung Hsing University, Taiwan.

**Author Contributions:** Tzu-Ken Lin and Dong-Sing Wu proposed the concept. Tzu-Ken Lin and Wei-Kai Wang conceived and designed the experiments. Tzu-Ken Lin, Shih-Yung Huang and Chi-Tsung Tasi contributed the films measurement results. Tzu-Ken Lin, Wei-Kai Wang and Dong-Sing Wu wrote the manuscript. All authors read and approved the final version of the manuscript to be submitted.

**Conflicts of Interest:** The authors declare no conflict of interest.

## References

1. Zavareh, M.A.; Sarhen, A.A.D.M.; Razak, B.B.; Basirun, W.J. Plasma thermal spray of ceramic oxide coating on carbon steel with enhanced wear and corrosion resistance for oil and gas applications. *Ceram. Int.* **2014**, *40*, 14267–14277. [[CrossRef](#)]
2. Kim, D.M.; Kim, K.B.; Yoon, S.Y.; Oh, S.Y.; Kim, H.T.; Lee, S.M. Effects of artificial pores and purity on the erosion behaviors of polycrystalline  $\text{Al}_2\text{O}_3$  ceramics under fluorine plasma. *J. Ceram. Soc.* **2009**, *117*, 863–867. [[CrossRef](#)]
3. Cardinaud, C.; Peignon, M.C.; Tessier, P.Y. Plasma etching: principles, mechanisms, application to micro- and nano-technologies. *Appl. Surf. Sci.* **2000**, *164*, 72–83. [[CrossRef](#)]
4. Cunge, G.; Inglebert, L.; Joubert, O.; Vallier, L.; Sadeghi, N. Ion flux composition in  $\text{HBr Cl}_2/\text{O}_2$  and  $\text{HBr}/\text{Cl}_2/\text{O}_2/\text{CF}_4$  chemistries during silicon etching in industrial high-density plasmas. *J. Vac. Sci. Technol.* **2002**, *20*, 2137–2148. [[CrossRef](#)]
5. Fukumoto, H.; Fujikake, I.; Takao, Y.; Eriguchi, K.; Ono, K. Plasma chemical behavior of reactants and reaction products during inductively coupled  $\text{CF}_4$  plasma etching of  $\text{SiO}_2$ . *Plasma Sources Sci. Technol.* **2009**, *18*, 045027. [[CrossRef](#)]
6. Ito, N.; Moriya, T.; Uesugi, F.; Matsumoto, M.; Liu, S.; Kitayama, Y. Reduction of particle contamination in plasma-etching equipment by dehydration of chamber wall. *Jpn. J. Appl. Phys.* **2008**, *47*, 3630–3634. [[CrossRef](#)]
7. Sato, N.; Uchida, G.; Kaneko, T.; Shimizu, S.; Iizuka, S. Dynamics of fine particles in magnetized plasmas. *Phys. Plasmas* **2001**, *8*, 1786–1790. [[CrossRef](#)]
8. Kim, D.M.; Lee, S.H.; Alexander, W.B.; Kim, K.B.; Oh, Y.S.; Lee, S.M. X-Ray photoelectron spectroscopy study on the interaction of yttrium–aluminum oxide with fluorine-based plasma. *J. Am. Ceram. Soc.* **2011**, *94*, 3455–3459. [[CrossRef](#)]
9. Qin, X.P.; Zhou, G.H.; Yang, H.; It Wong, J.; Zhang, J.; Luo, D.W.; Wang, S.W.; Ma, J.; Tang, D.Y. Fabrication and plasma resistance properties of transparent YAG ceramics. *Ceram. Int.* **2012**, *38*, 2529–2535. [[CrossRef](#)]
10. Iwasawa, J.; Nishimizu, R.; Tokita, M.; Kiyohara, M. Plasma-resistant dense yttrium oxide film prepared by aerosol deposition process. *J. Am. Ceram. Soc.* **2007**, *90*, 2327–2332. [[CrossRef](#)]
11. Mun, S.Y.; Shin, K.C.; Lee, S.S.; Kwak, J.S.; Jeong, J.Y.; Jeong, Y.H. Etch defect reduction using  $\text{SF}_6/\text{O}_2$  plasma cleaning and optimizing etching recipe in photo resist masked gate poly silicon etch process. *Jpn. J. Appl. Phys.* **2005**, *44*, 4891–4894. [[CrossRef](#)]
12. Ramos, R.; Gunge, G.; Joubert, O.; Sadeghi, N.; Mori, M.; Vallier, L. Plasma/react walls interactions in advanced gate etching process. *Thin Solid Films.* **2007**, *515*, 4846–4852. [[CrossRef](#)]
13. Rueger, N.R.; Beulens, J.J.; Schaepkens, M.; Doemling, M.F.; Mirza, J.M.; Standaert, T.E.F.M.; Oehrlein, G.S. Role of steady state fluorocarbon films in the etching of silicon dioxide using  $\text{CHF}_3$  in an inductively coupled plasma reactor. *J. Vac. Sci. Technol.* **1997**, *15*, 1881–1889. [[CrossRef](#)]
14. Standaert, T.E.F.M.; Hedlund, C.; Joseph, E.A.; Oehrlein, G.S.; Dalton, T.J. Role of fluorocarbon film formation in the etching of silicon, silicon dioxide, silicon nitride, and amorphous hydrogenated silicon carbide. *J. Vac. Sci. Technol.* **2004**, *22*, 53–60. [[CrossRef](#)]

15. Schaepekens, M.; Standaert, T.E.F.M.; Rueger, N.R.; Sebel, P.G.M.; Cook, J.M. Study of the SiO<sub>2</sub>-to-Si<sub>3</sub>N<sub>4</sub> etch selectivity mechanism in inductively coupled fluorocarbon plasmas and a comparison with the SiO<sub>2</sub>-to-Si mechanism. *J. Vac. Sci. Technol.* **1999**, *17*, 26–37. [[CrossRef](#)]
16. Lin, T.K.; Wu, D.S.; Huang, S.Y.; Wang, W.K. Characteristics of yttrium fluoride and yttrium oxide coatings for plasma process equipment prepared by atmospheric plasma spraying. *Jpn. J. Appl.* **2016**, *55*, 162601. [[CrossRef](#)]
17. Cao, Y.C.; Zhao, L.; Luo, J.; Wang, K.; Zhang, B.P.; Yotoka, H.; Ito, Y.; Li, J.F. Plasma etching behavior of Y<sub>2</sub>O<sub>3</sub> ceramics: Comparative study with Al<sub>2</sub>O<sub>3</sub>. *App. Surf. Sci.* **2016**, *336*, 304–309. [[CrossRef](#)]
18. Kim, D.M.; Oh, Y.S.; Kim, S.; Kim, H.T.; Lim, D.S.; Lee, S.M. The erosion behaviors of Y<sub>2</sub>O<sub>3</sub> and YF<sub>3</sub> coatings under fluorocarbon plasma. *Thin Solid Films* **2011**, *519*, 6698–6702. [[CrossRef](#)]
19. Standaert, T.E.F.M.; Schaepekens, M.; Rueger, N.R.; Sebel, P.G.M.; Oehrlein, G.S.; Cook, J.M. High density fluorocarbon etching of silicon in an inductively coupled plasma: Mechanism of etching through a thick steady state fluorocarbon layer. *J. Vac. Sci. Technol.* **1998**, *16*, 239–249. [[CrossRef](#)]
20. Tatsumi, T.; Matsui, M.; Okigawa, M.; Sekine, M. Control of surface reactions in high-performance SiO<sub>2</sub> etching. *J. Vac. Sci. Technol.* **2000**, *18*, 1897–1902. [[CrossRef](#)]
21. Matsui, M.; Tatsumi, T.; Sekine, M. Observation of surface reaction layers formed in highly selective SiO<sub>2</sub> etching. *J. Vac. Sci. Technol.* **2001**, *19*, 1282–1888. [[CrossRef](#)]
22. Korzenski, M.B.; Lecoeur, P.; Mercey, B.; Chippaux, D.; Raveau, B. PLD-grown Y<sub>2</sub>O<sub>3</sub> thin films from Y metal: An advantageous alternative to films deposited from yttria. *Chem. Mater.* **2000**, *12*, 3139–3150. [[CrossRef](#)]
23. Moulder, J.F.; Stickle, W.F.; Sobol, P.E.; Bomben, K.D. *Handbook of X-ray Photoelectron Spectroscopy*; Physical Electronics: Eden Prairie, MN, USA, 1995; p. 10.
24. Pei, L.; Jiapi, Z.; Yuankun, Z.; Jiecai, H. Preparation and optical properties of sputtered-deposition yttrium fluoride film. *Nucl. Instrum. Methods Phys. Res.* **2013**, *307*, 429–433. [[CrossRef](#)]
25. Vickerman, J.C.; Gilmore, I.S. *Surface Analysis*, 2nd ed.; Wiley: New York, NY, USA, 2009; p. 53.
26. Cunge, G.; Pelissier, B.; Joubert, O.; Ramos, R.; Maurice, C. New chamber walls conditioning and cleaning strategies to improve the stability of plasma processes. *Plasma Sources Sci. Technol.* **2005**, *14*, 599–609. [[CrossRef](#)]
27. Zhong, H.X.; Hong, J.M.; Cao, X.F.; Chen, X.T.; Xue, Z.L. Ionic-liquid-assisted synthesis of YF<sub>3</sub> with different crystalline phases and morphologies. *Mater. Res. Bull.* **2009**, *44*, 623–628. [[CrossRef](#)]
28. Barve, S.A.; Jagannath; Mithal, N.; Deo, M.N.; Chand, N.; Bhanage, B.M.; Gantayet, L.M.; Patil, D.S. Microwave ECR plasma CVD of cubic Y<sub>2</sub>O<sub>3</sub> coatings and their characterization. *Surf. Coat. Technol.* **2010**, *204*, 3167–3172. [[CrossRef](#)]
29. Kim, D.M.; Jang, M.R.; Oh, Y.S.; Kim, S.; Lee, S.M.; Lee, S.H. Relative sputtering rates of oxides and fluorides of aluminum and yttrium. *Surf. Coat. Technol.* **2017**, *309*, 694–697. [[CrossRef](#)]
30. Levin, I.; Huang, Q.Z.; Lawrence, P.C.; Winnie, W.N. Non-quenchable chemical order-disorder phase transition in yttrium oxyfluoride YOF. *Eur. J. Inorg. Chem.* **2005**, *1*, 87–91. [[CrossRef](#)]
31. Miwa, K.; Takada, N.; Sasaki, K. Fluorination mechanisms of Al<sub>2</sub>O<sub>3</sub> and Y<sub>2</sub>O<sub>3</sub> surfaces irradiated by high-density CF<sub>4</sub>/O<sub>2</sub> and SF<sub>6</sub>/O<sub>2</sub> plasmas. *J. Vac. Sci. Technol.* **2009**, *27*, 831–835. [[CrossRef](#)]
32. Tsunoura, T.; Yoshida, K.; Yano, T.; Kishi, Y. Fabrication, characterization, and fluorine-plasma exposure behavior of dense yttrium oxyfluoride ceramics. *Jpn. J. Appl.* **2017**, *56*, 06HC02.

